Electron correlation during photoionization and relaxation of potassium and argon after *K*-shell photoexcitation

Marcus P. Hertlein, Hidehito Adaniya, Kyra Cole, Benedict Feinberg, Jason Maddi, Michael H. Prior, Ralf Schriel, and Ali Belkacem
Lawrence Berkeley National Laboratory, Berkeley, California 94720, USA
(Received 12 June 2004; published 4 February 2005)

We have measured the charge-state distributions of argon and potassium after ionization by photons with energies near the *K*-shell ionization threshold. Despite the similarity in core electron configurations, the two atoms show remarkable differences in the resulting distribution of ion charge states. The valence electron in potassium is rarely a spectator during core relaxation, and its presence enhances the loss of electrons excited into Rydberg levels or strongly reduces the recapture of slow photoelectrons during postcollision interaction.

DOI: 10.1103/PhysRevA.71.022702 PACS number(s): 32.80.Hd, 32.80.Fb

I. INTRODUCTION

The dynamics of inner-shell photoionization and the resulting relaxation of the excited atom are complicated by the collective response of all the electrons of the atomic target. Furthermore, this correlated response of all of the electrons in the atom couples the photoionization and relaxation processes. The core hole created by x-ray photoexcitation in an atom can relax through a variety of channels, a number of which involve electron ejection and ultimately result in a multiply charged ion. These relaxation channels consist of a cascade of decay processes such as fluorescence, Auger, and Coster-Kronig transitions, where the core hole cascades up to the outer electron shell as it gets filled in by higher-lying electrons. The individual decay steps are coupled and cannot always be separated from each other or even from the photoionization process itself. For example, postcollision interaction (PCI) effects often occur in Auger decays following near-threshold inner-shell photoionization of atoms. The PCI effect is caused by the sudden change of the Coulomb field that an initially ejected slower photoelectron experiences when overtaken by a faster Auger electron. The energy exchange between the two electrons can in some cases result in the recapture of the photoelectron. This effect was extensively studied in the inner-shell photoionization of noble gases (see, for example, [1,2]). Many PCI investigations studied the changes in the ion charge-state distribution when the photon energy is varied through the ionization edge [1,3,4]. Others used electron spectroscopy to probe the energy exchange between the photoelectron and the fast Auger electron [2,5–7].

In this paper we compare the different ion yields and charge-state distributions for potassium and argon after *K*-shell ionization with photon energies from about 100 eV below to about 100 eV above their respective *K*-shell edges. Though loosely bound, the potassium valence electron plays a major role in the ionization dynamics. Striking differences and surprising similarities are observed between the charge-state distributions, which can be traced to the interplay between the various processes (shake-up, correlation between the valence electron and the photoelectron, PCI, and double excitation). The resulting difference between argon and potassium sheds light on the overall excitation and relaxation processes and on the pre-edge and postcollision interaction effects.

Gomilšec *et al.* [8] reported that above the *K*-shell ionization edge of potassium, double excitations of the form $[1s4s]4p5s$ are resonant and contribute as much as 10% to the absorption cross section. In the first part of this paper we will present total ion yield measurements that are directly comparable to the absorption measurements of Gomilšec *et al.* In the second part we take the measurements one step further by systematically measuring the various ion yields as the photon energy is varied across the *K* edge of potassium. Berry *et al.* [9] reported a limited measurement of the charge-state distribution of potassium ions following *K*-shell photoionization. Their data show some similarities between the average charge state of argon and potassium. However, that measurement had a large background and was hindered by the technical difficulties associated with working with potassium and by their low target density. In the present work we overcame some of the difficulties associated with potassium and systematically measured the charge-state distribution of ions as the energy of the x rays is varied across the respective *K*-shell edges of the atoms.

II. EXPERIMENT

This experiment was performed at beamline 9.3.1 at the Advanced Light Source (ALS) at the Lawrence Berkeley National Laboratory. Light from a bending magnet was passed through a Si(111) double-crystal monochromator with approximately 1:7000 energy resolution and then focused to a 1-mm spot size at the interaction region in the center of a vacuum chamber. The interaction region contained the atomic sample, either argon from backfilling the target chamber or potassium from an effusive oven near the focus. It was located between two metal plates comprising the extraction field region of a time-of-flight (TOF) spectrometer (Fig. 1). The interaction region visible to the detector was constrained transversally by the diameter of the x-ray beam and longitudinally by the size of a hole in one of the extraction plates and was filled by the sample. This ensured similar interaction volumes for both samples. The spectrometer was operated in

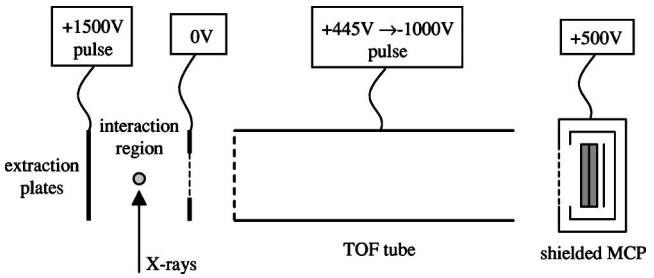

FIG. 1. Schematic of the experimental setup with time-of-flight (TOF) spectrometer used in pulsed field extraction mode. After initial accumulation period, both extraction plate and tube are pulsed to extract ions from the interaction region towards the microchannel plate (MCP). The MCP is enclosed by double shielding to minimize rf pickup. Dotted lines indicate grids.

pulsed ion extraction mode. During the initial accumulation phase of about 60 μs, the field plates were held at ground potential, allowing field-free accumulation of ions produced by the x rays. The drift tube behind the plates was held at a positive potential to prevent acceleration of background ions into the tube. During the extraction phase, a 110-ns-long, 740-V/cm extraction pulse was applied to the ions by biasing one of the field plates, while the drift tube was pulsed to −1000 V for about 1.2 μs, providing ion acceleration into the tube. The ions acquired significant kinetic energy during this extraction pulse, although the pulse was shorter than the time needed for any of the ions to reach the first extraction plate. This reduced the effects of initial position and thermal kinetic energy on the time of flight of the ions and, hence, the peak widths of the recorded signals, while assuring good collection efficiency. A rectangular hole in the field plate allowed only a restricted section of the ions produced along the x-ray beam path to enter the drift tube. Once all ions had entered the tube, the drift tube voltage was reverted to the original level, allowing the ions to exit the tube and accelerate towards the microchannel plate (MCP) detector. In order to avoid rejection of slower, lower-charge states, this voltage reversal should not occur too early. The minimum time delay for this phase could be determined by calculation or experimentally by adjustment until further delay did not result in any further increase in the 1+ charge-state yield. After the tube, the ions traversed a postacceleration field close to the MCP for increased detection efficiency of the ions. Although the effective detection efficiency inevitably varies slightly between different charge states due to collection and MCP detector efficiencies [10], between identical charges of the two elements the difference in total detection efficiency is presumably small, since argon and potassium have similar atomic masses and were recorded with identical experimental setup. The arrival time of the ions was measured with a multihit time-digital converter (LeCroy 3377TDC), with the trigger of the ion extraction pulse providing the common start of the time measurement.

The pulsing scheme allowed good separation of the ion charge states by keeping broadening of the ion peaks due to residual fields and thermal drift small, while still keeping the number of background ions low. Furthermore, when using the effusive oven source, the potassium vapor was directed

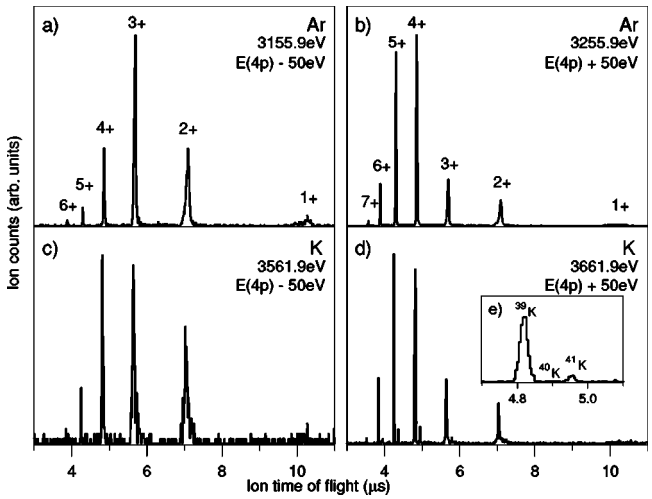

FIG. 2. Ion time-of-flight spectra for argon and potassium taken 50 eV below (a) and (c) and above (b) and (d) their respective 4*p* resonances. The vertical scales have been normalized to the height of the largest peak. Inset (e) shows a detail of (d), magnified to indicate the TOF isotope separation of potassium.

toward a large cooled metal plate for condensation. With this experimental setup, the MCP detector handled several days of continuous oven operation without the performance degradation or light sensitivity that is typical of potassium contamination. Apart from target density, the measurements with argon and potassium used identical parameters for the TOF spectrometer (such as voltages and timings) when recording the spectra, allowing a direct comparison of the data for the two atoms. The densities in the interaction region for both atoms were of order of 10^{11} atoms/cm^3.

Figure 2 shows TOF spectra for argon and potassium, taken at photon energies 50 eV above and below their respective 4*p* resonances. Both elements exhibit peaks corresponding to charge states 1+ through 8+. The background, mostly from stray energetic electrons, is more noticeable in the potassium spectra and in the spectra taken below the 4*p* resonance, because the lower count rate necessitated longer acquisition times. Virtually no counts, from oven operation or otherwise, were detected without the presence of x-ray photons.

The mode of operation of the TOF spectrometer and the narrow width of the ion peaks allowed the separation of the potassium isotopes, visible as separate peaks in the TOF spectrum in Fig. 2(e). The fractions of the isotope counts in our data for ^{39}K, ^{40}K, and ^{41}K, the three naturally occurring isotopes, were measured at (93±3)%, (0.2±0.1)%, and (6.5±0.7)%, respectively, and are consistent with the natural isotope abundances 93.26%, 0.0117%, and 6.73%. This attests for the almost background-free signal and high-charge-state resolution of the spectrometer.

III. RESULTS

A. Total ion yield

In this section we first present the total ion yield (obtained by adding the contribution from all the charge states from

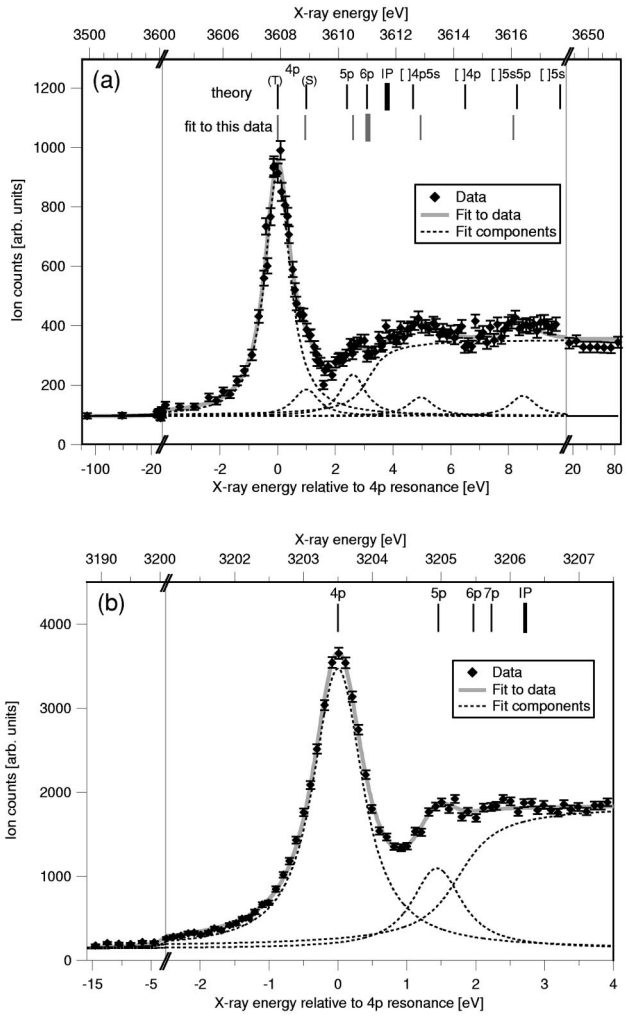

FIG. 3. Total ion yield from x-ray ionization of potassium (a) and argon (b). The thick solid gray line is a fit to the data, composed of a sum of resonance profiles and a step profile at the ionization edge (dashed lines). Table I lists positions and amplitudes of the fits. In this and subsequent figures, the short thin vertical lines indicate the positions of resonances from the literature [8,11] and short thick lines denote ionization limits. In the labeling of the resonances, square brackets denote a 1*s*4*s* double core hole. In this and subsequent figures, vertical light gray lines indicate a scale change in the *x* axis.

spectra similar to the ones shown in Fig. 2) as a function of the photon energy. Since we detect all ions simultaneously, our measurements of the total ion yield are directly comparable to the absorption measurements by Gomilšek *et al.* [8]. Figure 3 shows the total ion yield as a function of x-ray energy tuned around the *K*-shell ionization edge for potassium and argon. The potassium spectra are in very good agreement with x-ray absorption measurements reported by Gomilšek *et al.*, and the argon spectra are in equally good agreement with the results of Doppelfeld *et al.* [1] (total ion yield) and Breinig *et al.* [11] (absorption measurement).

The vertical bars at the top of Fig. 3 indicate the positions of resonances taken from literature. These references include experimental measurements for argon [11] and calculated

TABLE I. Position and relative amplitude of features in the potassium and argon spectra [Figs. 3(a) and 3(b), respectively], as determined by a least-squares fit. The energies are given relative to the 1*s*-4*p* resonances, 3607.9 eV for potassium and 3203.5 eV for argon, as are the amplitudes. Uncertainties in the fit amplitudes are less than 3% of the 4*p* height. The offset of the edge from the expected ionization potential is due to the combined overlap of higher-lying Rydberg resonances [8,11,12].

	Potassium		Argon	
Level	ΔE (eV)	I (%)	ΔE (eV)	I (%)
$[1s]4p$ $^{\text{triplet}}_{\text{singlet}}$	0.00 (5)	100	0	100
	1.00 (10)	11		
$[1s]5p$	2.60 (5)	17	1.45 (5)	28
Edge (fit)	3.15 (10)	32	1.75 (5)	52
IP (theory)	4		2.70	
$[1s4s]4p5s$	4.95 (15)	8		
$[1s4s]5s5p$	8.50 (20)	8		

Dirac-Fock energies for potassium [8], plotted relative to the 4*p* resonance. Figure 3 further shows the decomposition of the ion yield profile into a sum of individual resonance profiles, similar to a procedure outlined in Refs. [3,8]. Starting with Lorentzian resonance profiles (broadened by the monochromator transmission linewidth) and an arctangent ionization step function, we perform a least-squares fit to successive resonances to determine their widths, energy positions, and amplitudes from our data. For the fit, all the 1*s*-*np* resonances were assumed to have the same width, since their natural linewidths are mainly determined by the short lifetime of the 1*s* hole. Quantitative values of the positions and intensities of the various transitions, as determined by the fit, are summarized in Table I. They agree well with the calculated and measured values of Gomilšek *et al.* [8].

Both elements exhibit a large peak in the total ion yield at the 1*s*-4*p* excitation resonance. The resonances were probed by an x-ray beam with resolution of about 0.6 eV, which is less than the natural linewidth of the 1*s*-4*p* resonances (0.74 eV for potassium, 0.68 eV for argon). In potassium the 1*s*-4*p* transition is split into a dominant 4*p* triplet and a smaller 4*p* singlet seen in Fig. 3 as a right shoulder to the larger triplet transition. A smaller peak due to a 1*s*-5*p* excitation is also resolved through the fitting procedure. The higher states below the absorption edge overlap and cannot individually be resolved, which has the effect of an apparent shift of the ionization edge to lower energies in the spectrum. These states can hence be treated as part of the continuum states, following a procedure given by Teodorescu *et al.* [12] and Gomilšec *et al.* [8]

The total ion yield for potassium shows a clear enhancement above the ionization edge at the position of the $[1s4s]4p5s$ double-excitation resonance. Higher double-excitations of the form $[1s4s]4pnp$, which leave one electron in the 4*p* level, are reached at slightly higher photon energies and are visible as slight enhancements in Fig. 3(a). Their contribution decreases to the point of the $[1s4s]4p$ ionization limit where one electron enters the continuum. A similar

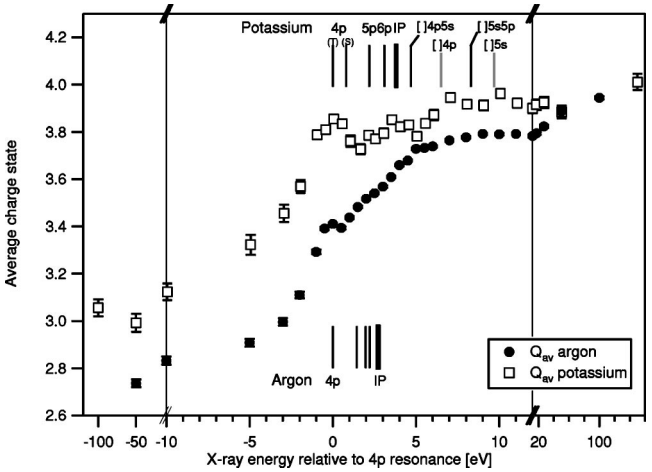

FIG. 4. The average charge Q_{av} of potassium and argon ions created by x-ray ionization. The spectra are aligned at the potassium 4*p* (triplet) and the argon 4*p* resonances.

yield enhancement is visible at the expected position of the $[1s4s]5snp$ Rydberg series. The ion yield towards the ionization limit of this series is not expected to decrease as it does in the $[1s4s]5pns$ case because higher-lying Rydberg series which fall into this region maintain the yield enhancements. Although peaks cannot be individually resolved here, it is possible to fit the $[1s4s]5s5p$ resonance to the start of this yield enhancement. At energies 50–100 eV above the 4*p* resonance no double-excitation resonances exist and the ion yield decreases back to a single-ionization level. As discussed below, here the photon only removes a single electron; the rest of the electrons are removed through relaxation of the *K* shell. Compared to this higher-energy region, in the region of the multiple-excitation resonances the ionization cross section is enhanced, due to the additional excitation pathway involving the 4*s* electron. For the $[1s4s]4p5s$ case, our fit shows that this increase is as high as 8% above the single-ionization cross section.

B. Average charge state

In this section we take one step further in our analysis and study how the charge-state distribution of the ions varies for potassium and argon as a function of the photon energy. The measurements for both atomic targets were performed in the same experiment using an identical setup, allowing a direct comparison of the charge-state distribution of the two elements.

First we focus on the average charge state Q_{av} produced in argon and potassium as the incident photon energy is varied around the *K*-shell ionization edge. Figure 4 shows Q_{av}, plotted for comparison purposes relative to the respective energies of the 1*s*-4*p* resonances of the elements. As expected, the average charge state for both atoms follows an increasing trend as the energy of the photon is increased through the *K*-shell ionization energy. However, we observe striking differences in the details of the average charge states that are directly related to the role that the additional 4*s* electron plays both in the ionization and relaxation processes.

We divide the average charge state spectrum into three major areas: Area 1 covers energies several eV below the 1*s*-4*p* transition, area 2 covers energies from the 1*s*-4*p* transition to several eV above the ionization edge, and area 3 covers energies well above the ionization edge. In all these areas the 4*s* electron in potassium plays an active role by being excited or ionized during the decay of a core hole. Ionization of this comparatively weakly bound valence electron leads to a charge state increased by 1, compared to argon going through a similar core-decay channel. In area 1 this effect is easily noticeable in the average charge state, which differs by more than 0.25 between argon and potassium at 50 eV below the 4*p* resonance. At such low photon energies, the main contribution to the average charge state comes from the decay of an *L*-shell hole, indicating that a significant fraction of the *L*-hole decay paths lead to concurrent shake-off of the 4*s* electron.

This is in contrast to what happens in area 3 far above the *K*-shell ionization edge. The average charge states of argon and potassium start to approach each other and reach similar levels 27 eV above 4*p*. At this energy, the average charge state is dominated by high-charge ions resulting from the relaxation of a *K*-shell hole. Unlike in area 1, the presence of the 4*s* electron in potassium does not create an increase in the charge state, meaning that the shake-off of the 4*s* electron is likely suppressed by the high charge of the core during relaxation.

In area 2, around the ionization *K*-shell edge, the photoelectron is either bound or has a low kinetic energy, resulting in a strong correlation with the 4*s*-electron. As a consequence we observe more complicated structures in the average charge state and large differences between potassium and argon. In the case of argon, the photoelectron is likely to stay bound to the final ion in the region between the 1*s*-4*p* transition and the *K*-shell ionization edge. The gradual rise of the average charge state above the ionization edge is due to the decreasing influence of the PCI effect, which results in a decreasing likelihood of recapturing the photoelectron through correlation with the outgoing *K-LL* Auger electron. This effect is extensively discussed in the literature [1–7]. The average charge state does not reach a plateau until 2.5 eV above the ionization potential, at which point the photoelectron is effectively lost. Beyond 15 eV above the ionization limit, the average charge state rises again as direct double ionization becomes possible in argon.

At the 4*p* resonance, potassium exhibits an average charge state 0.44 units higher than that of argon. The probable reason is that once the photoelectron is excited to the 4*p* state, which has the same major quantum number as the 4*s* valence electron, an extra *M-NN* Auger decay is possible that ejects the photoelectron. The net result is a higher average charge state for potassium than for argon. It is noteworthy that the gradual rise seen in argon for energies a few eV above the ionization potential (IP) is not seen for potassium. Instead the average charge state levels off just below the IP and continues rising only when resonances above the IP are reached. This points to major differences of the effects of the PCI on the charge-state distribution that can be attributed to the presence of a 4*s* valence electron in potassium. These differences are better reflected in the individual charge states, as we will show in the next section.

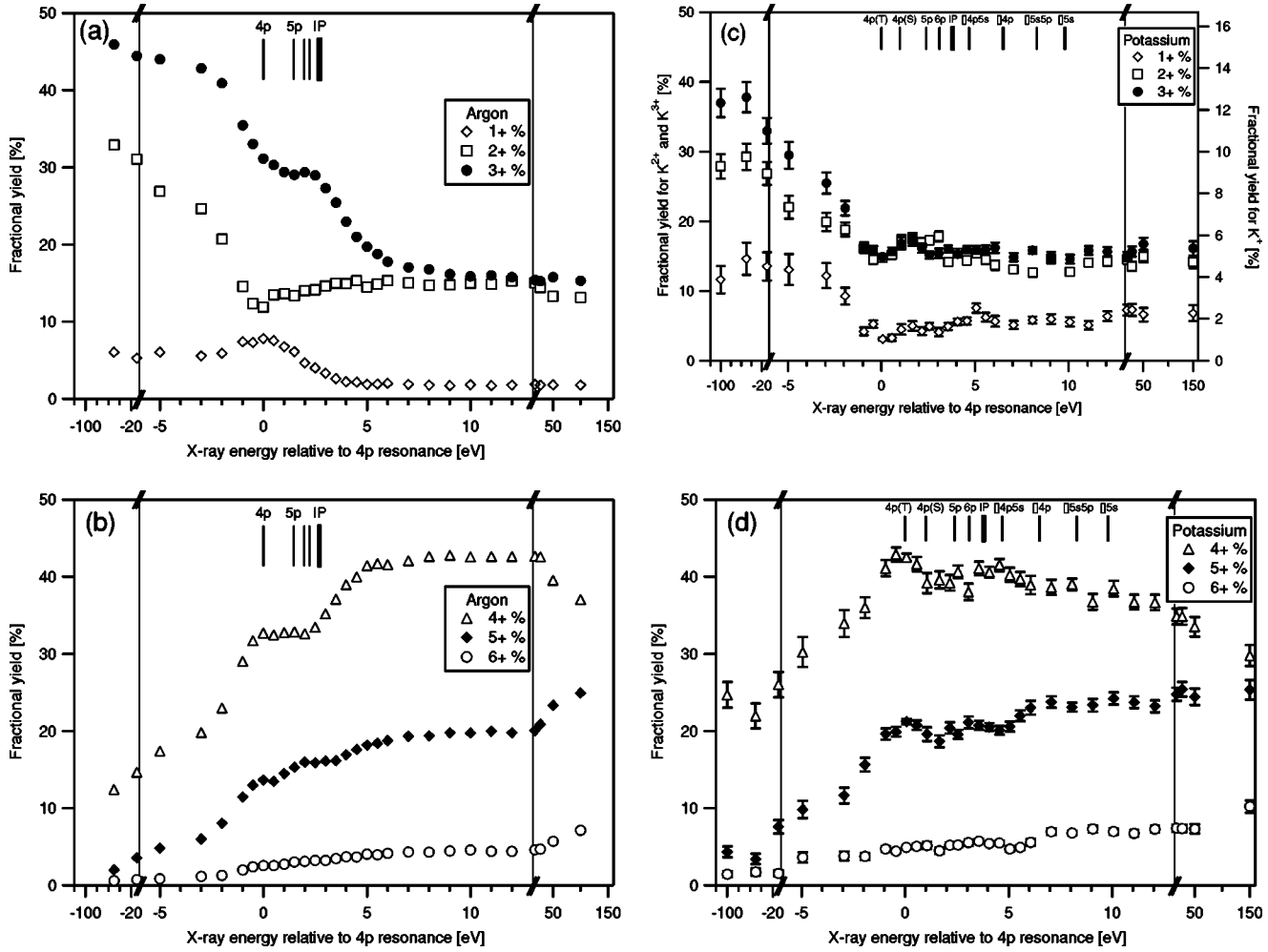

FIG. 5. Fractional ion yield for argon and potassium charge states 1+ through 6+. Note the different vertical scale for potassium 1+ in (c). Error bars for argon [(a) and (b)] are smaller than the size of the markers.

C. Charge-state yields

Figure 5 shows the production of ion charge states 1+ through 6+ for argon and potassium, expressed as a percentage of the total ion production. Rates and statistics for charge states 7+ and 8+ are low and are not plotted, and no higher charge states were detected. Here we will again divide the figure into three areas, areas 1, 2, and 3, encompassing photon energies below the 1*s*-4*p* resonance, between the 1*s*-4*p* transition and the IP, and above the IP, respectively. Our goal in this section is to try to gain more physical insight into various processes such as the PCI, pre-edge effect, and double excitations by comparing the change of individual charge states for argon and potassium in different areas.

One area of interest in Fig. 5 is just above the ionization threshold. Figures 5(a) and 5(b) show that in argon there is a gradual increase of charge state 4+ and a decrease of charge state 3+ with increasing photon energy. This "depopulation" of charge state 3+ in favor of charge state 4+ in argon, seen and reported in the literature [8], is interpreted as a direct effect of the PCI, in which the energy exchange between the fast Auger electron and the slow photoelectron can in some cases result in the recapture of the photoelectron. In the case of potassium, Figs. 5(c) and 5(d) do not exhibit a similarly striking change, suggesting that postcollision effects in potassium do not necessarily lead to a recapture of a slow photoelectron. The most likely source of this effect is the presence of the additional 4*s* electron in potassium, which can interact with the photoelectron during or after the ionization process, and prevent effective recapture through processes such as an *M-NN* Auger process.

Below the 1*s*-4*p* excitation, Figs. 5(a) and 5(c) show a gradual decrease of charge states 2+ and 3+ while Figs. 5(b) and 5(d) show a gradual increase of charge states 4+ and 5+ for argon and potassium. This monotonic increase or decrease of these charge states starts several tens of eV below the 1*s*-4*p* excitation. This effect is attributed by Amusia [13] to virtual 1*s*-4*p* excitation made energetically possible by borrowing energy from the subsequent Auger decay. The rate for this process is only appreciable for *K-LL* Auger decay, since the underlying core hole has to decay quickly in order to interact with the virtual excitation. This result is an ejected Auger electron, leaving the atom with an energy reduced by the amount that the photon lacks for direct 1*s*-4*p* excitation.

In order to shed some light on this pre-edge effect we combined in Fig. 6 the fractional yield of Ar^+ and K^+ as a

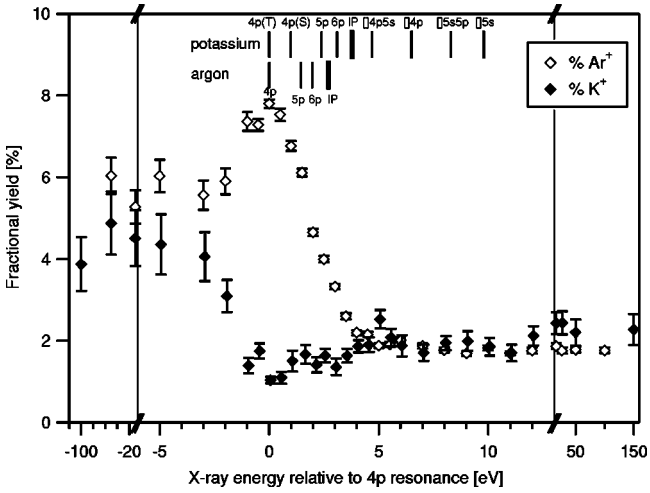

FIG. 6. Fractional ion yield comparison of potassium and argon singly charged ions.

function of the photon energy. As explained below, we observe two striking features in the 1+ fractional yields: the difference in behavior at the 4*p* resonance and the pre-edge behavior.

Our data show that slightly below the 1*s*-4*p* resonance, the 1+ fractional yield increases for argon but decreases for potassium with increasing photon energy; however, for each of the other charge states (2+ and above) the yields for the two elements track each other.

Furthermore, at low photon energies, far below the 4*p* resonance, the fraction of charge state 1+ is similar for argon and potassium, and does not change significantly with increasing photon energy until about 2 eV below the 1*s*-4*p* resonance. This is in contrast to charge states 2+ and above (Fig. 5), which show significant increases or decreases in that region. This means that the data show no pre-edge effect (associated with below-edge 1*s*-4*p* excitation and corresponding rise in yield) for charge state 1+.

This observation also rules out instrumental effects such as finite monochromator resolution, which could be a source of photons creating real 1*s*-4*p* excitations, as the source of this rise in yields of higher charge states, since otherwise all charge states, including 1+, should be affected and show corresponding changes.

The particular pathways that can lead to charge state 1+, both for potassium and argon, provide an explanation for the absence of the pre-edge effect for this charge state. Indeed, there are very few channels that can lead to charge state 1+, which makes the yield a sensitive indicator of the influence of the 4*s* valence electron of potassium on the ionization dynamics. Two dominant channels lead to singly charged argon or potassium: (a) direct *M*-shell photoionization, since no additional electrons besides the photoelectron are lost, and (b) *K*-shell excitation at photon energies near the *K*-shell ionization limit, where the photoelectron stays bound to the ion and the *K* hole is filled through a radiative transition from $n=2$ to $n=1$. (The probability for such *K*-*L* fluorescence is approximately 12% for argon and slightly higher for potassium [14,15].) The subsequent *L*-shell decay accounts for the loss of the single electron.

Note that direct *L*-shell ionization does not usually lead to singly charged argon or potassium, because the photoelectron is lost and the probability of *L*-*M* fluorescence is negligible (less than 0.15% [16,17]). Similarly, *K*-shell ionization by photon energies far above the IP removes the photoelectron and ultimately leads to an *L*-shell hole with associated additional electron loss.

The major observation here is that in both potassium and argon, a 1+ charge state can, for the most part, only be produced in the absence of a *K*-shell Auger process. The absence of the *K*-*LL* Auger decay path also eliminates the fast Auger electron that makes possible pre-edge (virtual) 1*s*-4*p* excitation and the associated slow ion yield rise several tens of eV below the resonance. According to this reasoning, the 1+ charge state, lacking this pathway, should therefore not exhibit a pre-edge effect, a behavior supported by our data (Fig. 6). This is not true for the higher-charge states, since the *K*-*LL* decay pathway is available; consequently, all of the charge state yields 2+ and higher do show the pre-edge change. This is a strong experimental indication that the pre-edge effect reported in the literature is a result of a correlation between the photoelectron and the fast *K*-*LL* Auger electron.

The fractional yield of Ar^+ shown in Fig. 6 has a maximum at the 4*p* excitation. As mentioned above, the rise results from the additional *K*-excitation channel becoming possible, with associated *K*-hole fluorescence and *L*-*MM* Auger decay with single-electron loss. In order for a significant Ar^+ yield to result from this cascade, the electron that was left in the 4*p* level from the initial core excitation must remain bound with significant probability during the relaxation processes of the core. In contrast to Ar^+, K^+ exhibits a minimum at the 4*p* resonance, indicating that potassium, relaxing through the same *K*-shell fluorescence channel, sheds an extra electron with a high probability. A likely explanation is that the photoelectron initially excited to the 4*p* state is ejected from the ion, with sufficient probability to deplete the singly charged-state yield, through an additional *M*-*NN* Auger process in which the 4*s* valence electron relaxes into one of the *M*-shell holes that appear after core relaxation.

The variation of the charge-state 1+ yield as a function of photon energy is also a very sensitive indicator of the correlation effects between the photoelectron and the 4*s* valence electron during both the ionization process and the relaxation process. An interesting feature in Fig. 6 is the increase of the fractional 1+ yield for potassium 5 eV above the 1*s*-4*p* excitation energy. This is the area where double excitation $[1s4s]4p5s$ contributes about 10% to the total cross section as reported in Table I, suggesting that the "excited" singly charged ion with two valence electrons in 4*p* and 5*s* has a sizable probability of relaxation without ejection of an additional electron. A further indication of the reduced electron loss of the $[1s4p]4p5s$ state of potassium is seen in Fig. 7, showing the fractional yield of K^{6+} and Ar^{6+} as a function of photon energy. The K^{6+} yield exhibits reductions at the double-excitation resonance, but otherwise rises monotonically towards higher energies. In contrast to potassium, Ar^{6+} exhibits a monotonic increase without any noticeable feature.

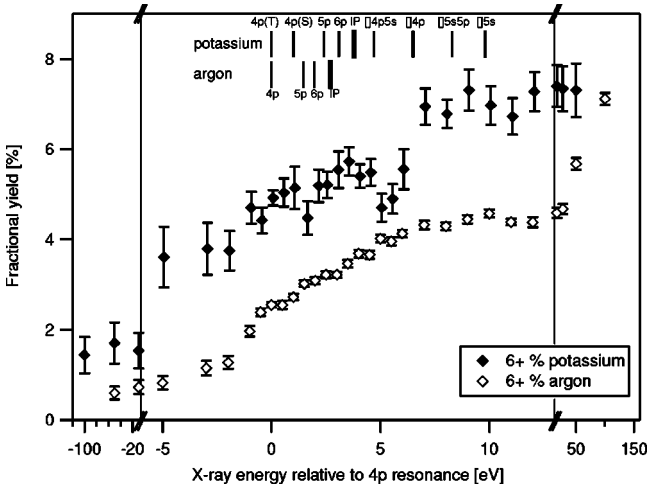

FIG. 7. Fractional ion yield comparison of potassium and argon 6+ ions.

This is a rather surprising result, considering the high probability of ejecting a photoelectron that has been excited to 4*p* while the 4*s* electron remains in the 4*s* level during the ionization process. Note that at very high energies both fractional 6+ yields of potassium and argon reach the same value of 7%.

IV. CONCLUSION

We have measured the charge-state distribution of argon and potassium resulting from photoionization with energies near the *K*-shell resonance. The presence of the 4*s* electron in potassium, with a core configuration otherwise identical to argon, has a strong influence on the ionization dynamics during the decay of a core hole. The valence electron is rarely a spectator during core relaxation, and its presence enhances the loss of electrons excited into Rydberg levels or strongly suppresses the recapture of slow photoelectrons through the PCI.

The influence of the valence electron is distinctly observable in the fractional ion yield of K^+, which is strongly suppressed at the 1*s*-4*p* resonance energy, in stark contrast to the Ar^+ yield. This indicates that the valence electrons have a high ionization probability and that *K*-shell excitation rarely leads to K^+. At the 4*p* resonance, most potassium charge states reach a fractional yield close to their high-energy limit and any PCI effect is minimal.

ACKNOWLEDGMENT

This work was supported by the Office of Science, Office of Basic Energy Sciences, Chemical Sciences Division of the U.S. Department of Energy (DOE) under Contract No. DE-AC-03-76SF00098.

[1] J. Doppelfeld, N. Anders, B. Esser, F. von Busch, H. Scherer, and S. Zinz, J. Phys. B **26**, 445 (1993).
[2] T. Hayaishi, E. Murakami, Y. Morioka, E. Shigemasa, A. Yagishita, and F. Koike, J. Phys. B **27**, L115 (1994).
[3] D. V. Morgan, R. J. Bartlett, and M. Sagurton, Phys. Rev. A **51**, 2939 (1995).
[4] G. B. Armen, J. C. Levin, and I. A. Sellin, Phys. Rev. A **53**, 772 (1996).
[5] J. C. Levin, C. Biedermann, N. Keller, L. Liljeby, C. S. O, R. T. Short, I. A. Sellin, and D. W. Lindle, Phys. Rev. Lett. **65**, 988 (1990).
[6] J. A. R. Samson, Y. Lu, and W. C. Stolte, Phys. Rev. A **56**, R2530 (1997).
[7] H. Kjeldsen, T. D. Thomas, P. Lablanquie, M. Lavollée, F. Penent, M. Hochlaf, and R. I. Hall, J. Phys. B **29**, 1689 (1996).
[8] J. Padežnik Gomilšec, A. Kodre, I. Arčon, and R. Prešeren, Phys. Rev. A **64**, 022508 (2001).
[9] H. G. Berry, Y. Azuma, P. L. Cowan, D. S. Gemmell, T. LeBrun, M. Ya Amusia, Nucl. Instrum. Methods Phys. Res. B **98**, 25 (1995).
[10] L. Pibida, R. Wehlitz, J. Levin, and I. Sellin, Nucl. Instrum. Methods Phys. Res. B **155**, 43 (1999).
[11] M. Breinig, M. H. Chen, G. E. Ice, F. Parente, B. Crasemann, and G. S. Brown, Phys. Rev. A **22**, 520 (1980).
[12] C. M. Teodorescu, R. C. Karnatak, J. M. Esteva, A. El Afif, and J-P. Connerade, J. Phys. B **26**, 4019 (1993).
[13] M. Ya Amusia, Phys. Lett. A **183**, 201 (1993).
[14] M. O. Krause, J. Phys. Chem. Ref. Data **8**, 307 (1979).
[15] K. Ueda, E. Shigemasa, Y. Sato, A. Yagishita, M. Ukai, H. Maezawa, T. Hayaishi, and T. Sasaki, J. Phys. B **24**, 605 (1991).
[16] S. Brünken, Ch. Gerth, B. Kanngießer, T. Luhmann, M. Richter, and P. Zimmermann, Phys. Rev. A **65**, 042708 (2002).
[17] M. O. Krause, Phys. Rev. A **22**, 1958 (1980).